Intelligent Automation And Soft Computing, 2019

Vol. 25, no. 3, 459–471
https://doi.org/10.31209/2018.100000001

Balanced GHM Mutiwavelet Transform Based Contrast Enhancement Technique for Dark Images Using Dynamic Stochastic Resonance

S. Deivalakshmi*, P. Palanisamy[1] and X. Z. Gao[2]

*,1 Department of Electronics and Communication Engineering, National Institute of Technology, Tiruchirappalli- 620015, Tamilnadu, India.
[2] School of Computing, University of Eastern Finland, Kuopio, Finland

ABSTRACT
The main aim of this paper is to propose a new technique for enhancing the contrast of dark images using Dynamic Stochastic Resonance (DSR) and Multi Wavelet Transform (MWT), which is computationally more efficient than the conventional methods. In the work, for enhancing the contrast of dark images, the intrinsic noise (darkness) of dark images has been used. The proposed MWT-based DSR scheme (MWT-DSR) can yield better performances in terms of visual information and color preservation than already reported techniques. The desired output response is validated by the Relative Contrast Enhancement Factor (F), Perceptual Quality Measures (PQM) and Color Enhancement Factor (CEF).

KEY WORDS: Complex Daubechies Wavelet Transform (CDWT), Contrast enhancement, Color Enhancement Factor (CEF), Discrete Wavelet Transform, Dynamic stochastic resonance, Multi Wavelet Transform (MWT), Perceptual Quality Measures (PQM), Relative Contrast Enhancement Factor (F).

1 INTRODUCTION

IMAGE enhancement is usually required for better visualization of dark images to improve feature identification, visual perception, and interpretability. Traditionally, noise is considered as an unwanted signal, which degrades the performance of a system. Stochastic resonance is a phenomenon, in which noise can be utilized to enhance rather than degrading the system performance. The first experiment on stochastic resonance for image visualization is reported in Simonotto, et al. (1997). Some of the recent work on the applications of stochastic resonance for grayscale images or edge enhancement has been published in Ye, et al. (2003); Hongler, et al. (2003); Ye, et al. (2004); Peng, et al. (2007); Rallabandi (2008); Rallabandi and Roy (2010); Ryu, et al. (2011).

Many of the existing contrast enhancement techniques in spatial domain are explained in Lim (1990); Gonzales and Woods (1992); Jobson, et al. (1997); Wolf, et al. (1998). Generally, the performance of a non-dynamic stochastic resonance based system can be improved by addition of external noise. The work proposed in this paper is completely different from these approaches. The technique in Peng, et al. (2007) and Ryu, et al. (2011) use the concept of non-dynamic stochastic resonance that adds N parallel frames of independent and identically distributed (i.i.d.) Gaussian noise and addition of external noise. The technique dealing with edge detection using vibrating noise is reported in Hongler, et al. (2003). The scheme developed for sonar image enhancement suggests the addition of external noise on bi-leveled images Ye, et al. (2004). The techniques on suprathreshold stochastic resonance Jha, et al. (2012); Jha, et al. (2012) deal with noise induced contrast enhancement of dark images. In a word, all these approaches work in spatial domain. Numerous applications of Stochastic Resonance (SR) for contrast enhancement are explored by addition of external noise, and the performance metrics are chosen based on experimentation. However, in the proposed technique, the intrinsic noise (darkness) present in an image due to low illumination has been utilized to enhance the contrast of the image.

Although many algorithms available in literature have been designed in block DCT domain for both colored and grayscale images Bockstein (1986); Mukherjee and Mitra (2008); Strickland, et al. (1987); Tang, et al. (2003), there are some drawbacks in

CONTACT S. Deivalakshmi deiva@nitt.edu

processing images using block DCT. As a matter of fact, using these algorithms processing the blocks independently is difficult due to the presence of blocking artifacts in the processed data. Sometimes, superfluous edges may appear at the image boundaries due to the sharp discontinuities of the intensity distribution. Therefore, the DWT based image enhancement using DSR has been proposed in Rajlaxmi Chouhan, et al (2012). In this paper, the Multi Wavelet Transform (MWT) based contrast enhancement technique has been proposed so as to avoid blocking artifacts. The low and the high frequency informations are processed simultaneously by means of the Dynamic Stochastic Resonance (DSR) model. The proper preservation of color is achieved by processing on the intensity vector of saturation model. In the proposed technique, an analogy to Benzi's double well model for recurrence of ice ages Benzi, et al (1981) is presented in the Multi Wavelet transform (MWT) domain. The proposed technique selects the double well parameters by the maximization of the SNR, and also relates the DSR parameters with the statistical properties of the poorly illuminated image itself.

Color image filtering methods for variable spray systems were discussed in Huihui, et al (2012). Four color image filtering algorithms were tested in the color images according to the noise characteristics. The test results revealed the fact that the filter based on RGB scalar had poor effect because of the appearance of some new colors, and it was the slowest; the rest filters nearly had no difference, and the filter based on RGB vector was the fastest. For efficient gray scale and RGB image denoising, smart real time adaptive gaussian filter supervised neural network is presented in Hassene Seddik, et al (2014). To target and eliminate different kinds and densities of noise in the image, neural networks are used for transforming static Gaussian low-pass filter to dynamic smart filter. Simulation results shows that the proposed method is able to filter efficiently corrupted data and reduce noise as well as preserve edges and forms.

The rest of this paper is organized as follows. Section 2 and 3 review the undecimated multiwavelet and complex daubechies wavelet transforms. Section 4 briefs the concept of DSR and its mathematical formulation. Section 5 further presents the proposed enhancement algorithm. The experimental results are discussed in Section 6. Section 7 finally draws the conclusions of the paper, and provides a few remarks.

2 MULTI WAVELET TRANSFORM (MWT)

THE scalar wavelets have a single scaling function $\phi(t)$ and wavelet function $\psi(t)$, whereas multiwavelets may have two or more wavelet and scaling functions Strela, et al (1999); Vasily Strela (1996). There are two types of multiwavelets. They are balanced multi wavelets and unbalanced multi wavelets. In the unbalanced multiwavelets, due to the application of the filter coefficients on the images, the boundaries are not treated properly, as they have dissimilar spectral characteristics of sub bands. Therefore, the pre-processing step is required to treat the image boundaries effectively before applying the filter coefficients Lahouari Ghouti, et al. (2006). Unfortunately, this pre filter (pre-processing filter) phase may destroy the properties that a multiwavelet basis is designed to have Selesnick (2000). The balanced multiwavelet eliminates the use of pre-filtering, and they are computationally more efficient than the unbalanced multiwavelet. The multiwavelet decomposition iterates on the low-frequency components generated by the previous decomposition level. After the first level scalar wavelet decomposition, the single low frequency sub band is present, whereas in the multiwavelet decomposition, r^2 low frequency components are present. The next iteration continues to decompose the low frequency sub bands (L_oL_0, L_0L_1, L_lL_o, L_1L_1). In this situation, when r=2, a structure of 4(3*J+1) sub bands can be generated after the J^{th} decomposition. When for J=1, the decomposition is shown in Figure 1.

The 'r' scaling functions can be written using the following vector notation.

$$\phi(t)=[\phi_1(t)\ \ \phi_2(t)\ \ \phi_3(t)\ldots\ldots..\phi_r(t)]^T \tag{1}$$

where $\phi(t)$ is called the multi scaling function.

In the same way, the 'r' wavelet functions can be represented as follows:

$$\psi(t)=[\ \psi_1(t)\ \ \psi_2(t)\ \ \psi_3(t)\ldots..\ \psi_r(t)]^T \tag{2}$$

In general, a scalar wavelet is represented with r=1. Most of the developed multiwavelet transforms use two scaling and wavelet functions, but theoretically r can take any value. Similar to the scalar wavelets, for r=2, the multi scaling function satisfies the following two scale equations

$$\phi(t) = \sqrt{2}\sum_{-\infty}^{\infty} H_k \phi(2t-k) \tag{3}$$

$$\psi(t) = \sqrt{2}\sum_{-\infty}^{\infty} G_k \phi(2t-k) \tag{4}$$

where H_k and G_k are 2x2 matrix filters defined as:

$$H_k = \begin{pmatrix} h_o(2k) & h_o(2k+1) \\ h_1(2k) & h_1(2k+1) \end{pmatrix} \quad G_k = \begin{pmatrix} g_o(2k) & g_o(2k+1) \\ g1(2k) & g_1(2k+1) \end{pmatrix} \tag{5}$$

The matrix elements actually provide more degrees of freedom than a traditional scalar wavelet. These extra degrees of freedom are employed to incorporate useful properties into the multiwavelet filters, e.g., symmetry, orthogonality and high order of approximation. The multiwavelet transform is implemented through a filter bank structure as shown in Figure 2. $L_0(z)$ and $L_1(z)$ are the transforms of the

two low pass branch filters L_0 and L_1. Similarly, $H_0(z)$ and $H_1(z)$ are the transforms of the two high pass branch filters H_0 and H_1. In the time varying filter bank implementation, the coefficients of the two low pass branch filters L_0 and L_1. Similarly, $H_0(z)$ and $H_1(z)$ are the transforms of the two high pass branch filters H_0 and H_1. In the time varying filter bank implementation, the coefficients of the two low pass and high pass filters are simply interleaved at the output. However, in the 2-D transform case with r=2, a total 16 sub bands are obtained instead of the usual four sub bands with scalar wavelet transforms.

L_0L_0	L_0L_1	L_0H_0	L_0H_1
L_1L_0	L_1L_1	L_1H_0	L_1H_1
H_oL_o	H_oL_1	H_oH_o	H_oH_1
H_1L_o	H_1L_1	H_1H_o	H_1H_1

Figure 1. Sub band distribution structure for first level MWT decomposition.

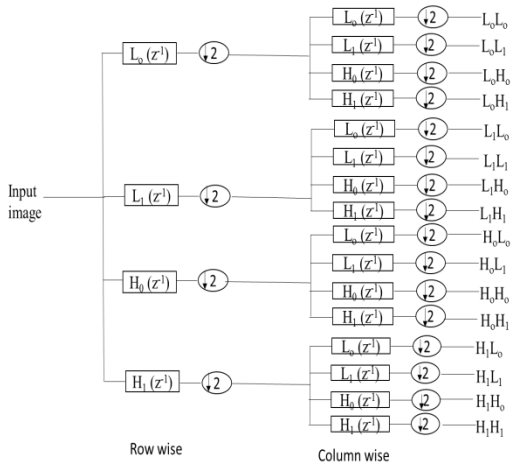

Figure 2. MWT decomposition.

For the second level decomposition, one should apply the MWT over four low frequency sub bands, which can be obtained after the first level decomposition. The scaling and wavelet coefficients for the GHM balanced multi wavelet are tabulated in Table 1.

3 COMPLEX DAUBECHIES WAVELET TRANSFORM (CDWT)

AS we know that the wavelets form bases, in which a signal can be decomposed using multi resolution analysis into a wide range of scales. It allows the detection of short lived time components, which need high time resolution as compared with the low-frequency components, where a detailed frequency analysis is often desired. The Discrete Wavelet Transform (DWT) can decompose a signal in its time domain into time frequency domain with the expression of a set of translated and scaled version of a basis mother wavelet Rao and Bopardikar (2000) using a set of functions, such as wavelet scaling function $\psi(t)$ and wavelet function $\phi(t)$ in the time domain with real-valued coefficients associated with high pass and low pass filters respectively. The wavelet decomposition enables the signal to pass through a series of complementary high pass filters as well as low pass filters separately, and can be down sampled by two for generating the higher frequency (details components) and lower frequency coefficients (approximation component).

On the other hand, the real-valued DWT have some disadvantages, such as lack of phase information and symmetry. It has been proved that complex solutions do exist leading to the Complex Daubechies Wavelet Transform (CDWT), which is a natural extension of the concepts of the Daubechies real-valued wavelet transform. In the CDWT, the complex valued filters are used instead of real filters, which can provide high degree of shift invariance and phase information Lina and Mayrand (2002). The construction of the CDWT can be achieved through the use of multi resolution analysis Lina (1997).

For Daubechies wavelet, let $h(z) = \frac{1}{2}(1+z)$ for the following polynomial:

$$p_N(z) = \sum_{k=0}^{N} (-1)^k \frac{2N+1}{k} h(z)^{2N-2K} h(z)^{2k} \tag{6}$$

which satisfies $\boldsymbol{P_N(Z) - P_N(-Z) = Z}$, when $\boldsymbol{Z_m}$ m= 1, 2, 3, ….J. The set of roots of $\boldsymbol{P_J(z)}$ inside the unit circle ($|\boldsymbol{Z_m}|<1$), and any selection of R among the roots $\boldsymbol{P_J(z)}$ defines an admissible trigonometric polynomial that satisfies the constraints of multi resolution analysis:

$$F(z) = h(z)^{1+N} \prod_{m\in\Re} \frac{z^{-1} - z_m}{1 - z_m} \times \prod_{n\notin\Re} \frac{z^{-1} - \overline{Z^{-1}_n}}{1 - Z^{-1}_n} \tag{7}$$

The solutions of Eqs. (6) and (7) give us the Daubechies scaling functions with real as well as complex valued coefficients. Any function *f(x)* can be decomposed into a complex scaling function and a mother wavelet as

$$f(x) = \sum_k c_k^{j_0} \varphi_{j_0 k}(x) + \sum_{j=j_0}^{\infty} \sum_k d_k^j \psi_{j,k}(x) \tag{8}$$

Table 1. Scaling and Wavelet Filter Coefficients

L_0	L_1	H_0	H_1
0.01513026672650	0.00044873488326	0.00666766359674	-0.00044873488326
-0.10232198801947	0.01089896516162	0.10321945778598	-0.01089896516162
0.10232198801947	-0.00303467520953	0.04509164359067	0.00303467520953
0.69197651446004	-0.07370681580507	-0.069804586487911	0.07370681580507
0.69197651446004	0.07415555068833	0.069804586487911	0.13138589511713
0.10232198801947	0.69924249123446	-0.04509164359067	-0.69077988810469
-0.10232198801947	0.69924249123446	-0.10321945778598	0.69077988810469
0.01513026672650	0.07415555068833	-0.00666766359674	-0.13138589511713
0	-0.07370681580507	0	-0.07370681580507
0	-0.00303467520953	0	-0.00303467520953
0	0.01089896516162	0	0.01089896516162
0	-0.00044873488326	0	-0.00044873488326

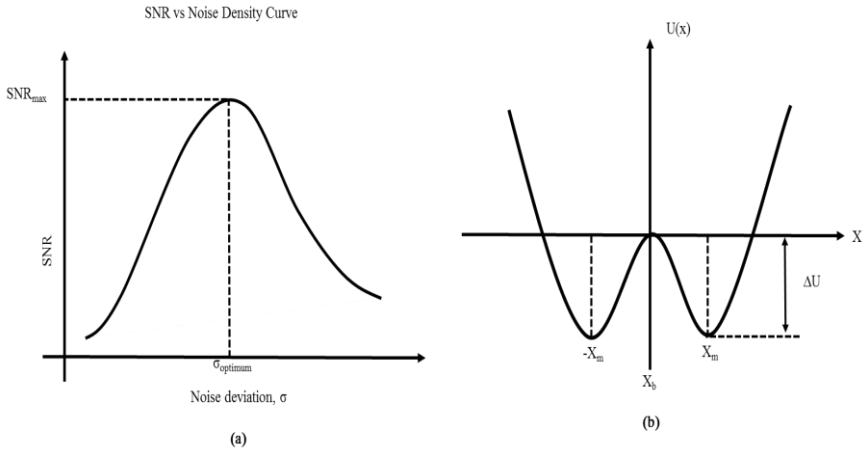

Figure 3. (a) SNR vs noise standard deviation curve. The SNR is observed to follow a resonant nature. (b) Bistable double potential well with two stable states.

where j_0 is a given resolution level and

$$\left\{c_k^j\right\} = \left\langle \varphi_{j,k} \mid f \right\rangle$$

and

$$\left\{d_k^j\right\} = \left\langle \psi_{j,k} \mid f \right\rangle$$

are approximation and detail coefficients, respectively. Equation (8) can be generalized to two dimensional signal *f(x, y)* as

$$f(x,y) = \sum_{m,n} c_{m,n}^{j_{\max}} \phi_{j_{\max} m,n}(x,y) \tag{9}$$

which can be expanded:

$$f(x,y) = \sum_k c_k^{j_0} \phi_{j_0,k}(x,y) + \sum_{j=j_0}^{j_{\max}-1} \sum_k d_{j,k}^0(x,y) \psi_{j,k}^0(x,y) + \sum_{j=j_0}^{j_{\max}-1} \sum_k d_{j,k}^1(x,y) \psi_{j,k}^1(x,y) + \sum_{j=j_0}^{j_{\max}-1} \sum_k d_{j,k}^2(x,y) \psi_{j,k}^2(x,y) \tag{10}$$

where the first term in equation is an approximate component of the input image signal, and the remaining three terms are detail components, i.e., horizontal, vertical, and diagonal components, respectively. The CDWT's low pass and high pass filter coefficients $h_0(n)$ and $h_1(n)$ are given in Table 2.

4 DYNAMIC STOCHASTIC RESONANCE AND ITS MATHEMATICAL FORMULATION

GENERALLY, noise is considered as an unwanted signal, which degrades the performance of a given system. However, recent studies have shown that in nonlinear systems, noise can be used to cause the amplification of weak signals, and can result in increase of signal to noise ratio. The SR occurs when SNR and input/output correlation have the maximum value at certain noise level. This concept is well explained in Rao and Bopardikar (2000). Any system to exhibit stochastic resonance should possess the following three properties like non-linearity in terms of threshold, sub threshold signals like signals with small amplitude, and a source of additive noise. This phenomenon occurs frequently in the bi stable systems Lina and Mayrand (2002). For the lower noise intensities, weak signal cannot cross threshold results in low SNR, and for the higher noise intensities, the output is dominated by noise, which again results in low SNR. At the moderate noise intensities, the signal to cross threshold results in the maximum SNR at the optimum noise level, as shown in Figure 3(a). We also have

$$\frac{dx(t)}{dt} = -\frac{dU(x)}{dx} + \sqrt{D}\xi(t) \tag{11}$$

U(x) in equation (11) is bi stable potential as shown in Figure 3(b), and is given in the following equation. ξ(t) is the additive zero mean stochastic fluctuation, and D is the noise variance.

$$U(x) = -\frac{ax^2}{2} + \frac{bx^4}{4} \tag{12}$$

From the above equation, *a* and *b* are double well parameters. The double well system is stable at $x = \pm\frac{\sqrt{a}}{b}$ separated by barrier of height $\Delta U = \frac{a^2}{4b}$, where ξ(t) =0.

Addition of periodic input signal $B\sin(\omega t)$ makes the bi stable system time dependent so that its dynamics are governed by the following equation:

$$\frac{dx(t)}{dt} = -\frac{dU(x)}{dx} + B\sin(\omega t) + \sqrt{D}\xi(t) \tag{13}$$

where ω and *B* are the frequency and amplitude of the input signal, respectively. It is assumed that the small amplitude of signal is not enough, and in the absence of noise, it is insufficient to move the particle from one well to other. By substituting equation (12) into equation (13), we have

$$\frac{dx(t)}{dt} = [ax - bx^3] + B\sin(\omega t) + \sqrt{D}\xi(t) \tag{14}$$

In the absence of the periodic force, the particle fluctuates around its local stable states. The rate of transition of particle (r_k) between potential well under noise driven switching is given by Kramer's rate Lina (1997), as in the following equation.

Table 2. CDWT Filter Coefficients

$h_0(n)$	$h_1(n)$
0.0105 + 0.0206i	0.0105 + 0.0206i
-0.0171 + 0.0087i	0.0171 - 0.0087i
-0.0806 - 0.1179i	-0.0806 - 0.1179i
0.1514 - 0.0942i	-0.1514 + 0.0942i
0.6430 + 0.1829i	0.6430 + 0.1829i
0.6430 + 0.1829i	-0.6430 - 0.1829i
0.1514 - 0.0942i	0.1514 - 0.0942i
-0.0806 - 0.1179i	0.0806 + 0.1179i
-0.0171 + 0.0087i	-0.0171 + 0.0087i
0.0105 + 0.0206i	-0.0105 - 0.0206i

$$r_k = \frac{a}{\sqrt{2\pi}} \exp\left(-\frac{2\Delta U}{D}\right) \tag{15}$$

Noise driven switching between potential well takes place when weak periodic force is applied to unit mass particle in potential well and is synchronized with the average waiting time $T_k(D) = \left(\frac{1}{r_k}\right)$ between two noise driven inter well transitions satisfying the time scale matching between the residence times of the particle in each well and signal frequency ω Gammaitoni, et al (1998).

$$2T_k(D) = T_\omega \tag{16}$$

T_ω is the period of periodic force. The most important factor in stochastic resonance is SNR. The expression for the SNR in the DSR as derived from [33] is given as

$$SNR = \left[\frac{4a}{\sqrt{2}(\sigma_0\sigma_1)^2}\right]\exp\left(-\frac{a}{2\sigma_0^2}\right) \tag{17}$$

where σ_0 is the standard deviation of the internal noise of the original bi stable system, and σ_1 is the standard deviation of added noise in the SR based system. The maximum SNR is acquired when the intrinsic parameter of dynamic double well system $a = 2\sigma_0^2$. The other parameters can be obtained from the parameter a, and for a weak signal, the sub threshold condition required is $b = \frac{4a^3}{27}$. Solving equation (14) using Euler Maruyama's iterative discretized method Risken (1984), we can obtain

$$x(n+1) = x(n) + \Delta t[ax(n) - bx^3(n) + input\,(n)] \tag{18}$$

where $input\,(n) = B\sin(\omega t) + \sqrt{D}\xi(t)$ denotes sequence of signal and noise, and Δt is the sampling time based on experimentation and initially $x(n) = 0$.

5 THE PROPOSED ENHANCEMENT ALGORITHM USING DSR AND MWT

THE major steps involved in the proposed method are given as follows.

Step 1. The low contrast colour input image is projected into the HSV color space to ensure inherent colour preservation of the image and to minimize the computation complexity.

Step 2. The Value vector (V) is decomposed into 16 sub bands (approximation and detail) using the analysis filter coefficients of the balanced multi wavelet transform as given in Table 1.

Step 3. The SR parameters are computed from all the 16 sub bands by assuming initial values for m, n and Δt. That is, x(0)=0, Δt=0.15 for gray images and $1 \leq \Delta t \leq 5$ for color images, $a_s = k \times 2\sigma_0^2$, $b_s = m \times 4(a_s^3)/27$, where s ϵ L_0L_0, L_0L_1, L_0H_0, L_0H_1, L_1L_0, L_1L_1, L_1H_0, L_1H_1, H_oL_o, H_oL_1, H_oH_o, H_oH_1, H_1L_o, H_1L_1, H_1H_o, H_1H_1. The bistable parameters a_s and b_s are computed for each of the 16 sub bands using its local variance (σ_{0s}^2). Here, m is a factor much less than 1 to ensure the sub threshold condition of the signal. k is a factor denoting the image region dullness, and is given as the inverse of (variance×dynamic range).

Step 4. Using the dynamic stochastic resonance parameters, the tuned multi wavelet transform sub band coefficients are found for all the 16 sub bands iteratively with the equation given in (19).

$$x(n+1) = x(n) + \Delta t[ax(n) - bx^3(n) + MWTcoeff\,] \tag{19}$$

Step 5. Inverse MWT is found for every iterated tuned set of the MWT coefficients using the synthesis filter coefficients.

Step 6. The conversion of the HSV color space to RGB is performed on the synthesized image to obtain the contrast enhanced image.

Step 7. Calculate F, PQM, and CEF for the contrast enhanced image.

For the second level MWT decomposition, the low frequency sub bands (L_oL_o, L_0L_1, L_lL_o, L_1L_1) obtained by the first level MWT decomposition is used. The second level MWT decomposition results 64 sub bands, in which a total of 16 sub bands are approximation sub bands, and the remaining 48 sub bands are detail sub bands. For the second level MWT based DSR, the above mentioned steps from 1 to 7 are performed on all the 64 sub bands. Similarly, the above steps are followed to analyse the performance of the DSR in complex daubechies wavelet domain by making use of filter coefficients given in Table 2. To enable the tuning step adaptive, iteration is continued until the sum of F(n)+CEF(n) becomes the maximum in the nearest possible vicinity of PQM = 10, e.g., 10 ± 2. For enhancing the low contrast gray scale images, the above steps are repeated except for Step 1 and 6, and, therefore, the MWT is directly applied on it. The block diagram representation of the above proposed algorithm is also shown in Figure 4. As the noise free image is required for measuring the metrics Mean Square Error (MSE) and Peak Signal to Noise Ratio (PSNR), and such images are not available here, the performance of the proposed enhancement technique cannot be analysed using the MSE and PSNR. Thus, to analyse the performance of the proposed technique, relative contrast enhancement factor (F), Perceptual Quality Metric (PQM) and Color Enhancement Factor (CEF) are applied in our simulations.

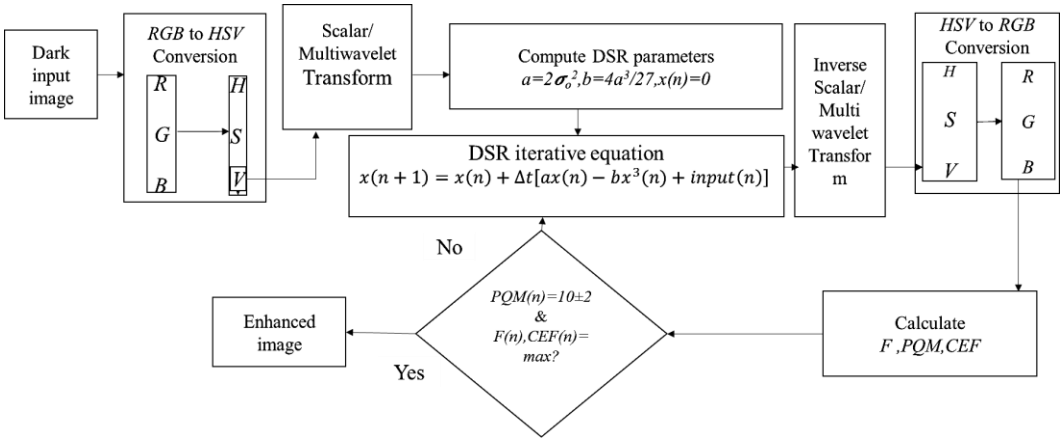

Figure 4. **Block diagram of the proposed algorithm.**

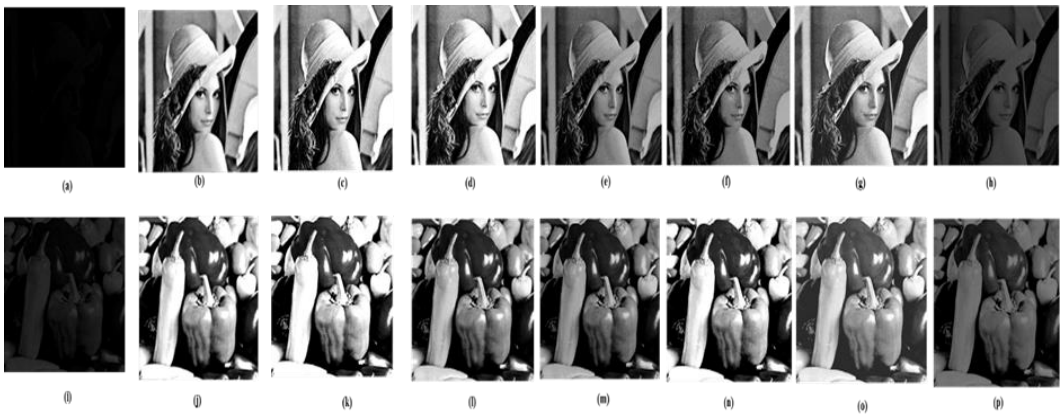

Figure 5. **Comparison of proposed method result with existing enhancement technique results for different dark gray images. (a), (i) -Input images, (b), (j) second level MWT based DSR method (c), (k) first level MWT based DSR method (d),(l)CDWT-DSR technique, (e), (m) DWT based DSR method (f),(n) DSR technique (g), (o) HEQ technique (h), (p) Gamma correction.**

5.1 Contrast enhancement factor (F)

The contrast enhancement (F) is based on global variance and mean of the original and enhanced images Rallabandi and Roy (2010). The no-reference Relative contrast enhancement factor, F, is calculated as the ratio of the values of the post enhancement Quality index (Q_B) and the pre-enhancement Quality index (Q_A). The Quality index $Q = \frac{\sigma^2}{\mu}$, where σ is the standard deviation, and μ is the mean of an image.

5.2 Color Enhancement Factor (CEF)

The Color Enhancement Factor (CEF) is defined as the ratio of the colorfulness of the enhanced and input images. The metric in terms of colors called colorfulness metric (CM) Mukherjee and Mitra (2008) is given as

$$CM(I) = \sqrt{\sigma_\alpha^2 + \sigma_\beta^2} + 0.3\sqrt{\mu_\alpha^2 + \mu_\beta^2} \quad (20)$$

where σ is the standard deviation, and μ is the mean of an image. We have α= R-G and β= (R+ (G/2))-B. R, G and B represent the red, green, and blue components of an image, respectively. Similarly, μ_α and μ_β are their means. The color enhancement factor (CEF) is defined as the ratio of colorfulness of the enhanced image (CM_E) to that of the original image (CM_I):

$$CEF = \frac{CM_E}{CM_I} \quad (21)$$

For the low contrast grayscale images, only F and PQM are measured after enhancement.

5.3 Perceptual quality metric (PQM)

Perceptual quality is a no reference metric used for judging the image quality taking into account the visible blocking and blurring artifacts Wang, et al.

(2002). The test image signal is denoted as x (m, n) for m∈ [1, M] and n∈ $[1, N]$, and the difference across each horizontal line is given as

$$d_h(m,n) = x(m,n+1) - x(m,n), n \in [1, N-1] \quad (22)$$

The blockiness is estimated as the average difference across the block boundaries:

$$B_h = \frac{1}{M([N/8]-1)} \sum_{i=1}^{M} \sum_{j=1}^{[N/8]-1} |d_h(i,8j)| \quad (23)$$

By combining the blockiness and activity, we can find the blurriness of an image. The activity is measured using two factors. The first is the average absolute difference between in-block image samples:

$$A_h = \frac{1}{7}\left[\frac{8}{M(N-1)} \sum_{i=1}^{M} \sum_{j=1}^{N-1} d_h(i,j) - B_h\right] \quad (24)$$

The second activity measure is the zero crossing (ZC) rate.

We here define for n ∈ $[1, N-2]$, $Z_h(m,n) =$

$$\begin{cases} 1 & horizantal\ ZC\ at\ d_h(m,n) \\ 0 & otherwise \end{cases} \quad (25)$$

The horizontal ZC rate can be estimated as

$$Z_h = \frac{1}{M(N-2)} \sum_{i=1}^{M} \sum_{j=1}^{N-2} Z_h(i,j) \quad (26)$$

$$A = \frac{A_h + A_v}{2}, \quad B = \frac{B_h + B_v}{2}, \quad Z = \frac{Z_h + Z_v}{2} \quad (27)$$

The good prediction performance called Perceptual Quality measure (PQM) is

$$PQM = \alpha + \beta B^{\gamma_1} A^{\gamma_2} Z^{\gamma_3} \quad (28)$$

where α, β, γ_1, γ_2 and γ_3 are the model parameters that are estimated with the subjective test data as described by (α = − 245.9, β = 261.9, γ_1 = − 0.0240, γ_2 = 0.0160 and γ_3= 0.0064)

6 EXPERIMENTAL RESULTS AND DISCUSSIONS

THE proposed method is implemented as an algorithm and tested on the very dark gray level and colored images. The results obtained using the proposed MWT based DSR technique (MWT-DSR) on colored and very dark grayscale images have been compared with the results obtained for various enhancement techniques, such as CDWT based DSR technique (CDWT-DSR), DWT based DSR technique (DWT-DSR) Rajlaxmi Chouhan, et al (2012), DSR Jha, et al. (2012), Histogram equalization (HEQ), Gamma correction Gonzales Woods (1992), Multiscale retinex (MSR) Jobson, (1997) and Retinex Jobson, et al. (1997). For the implementation of DWT-DSR method, in this work, the db1 wavelet is used. Figures 5 and 6 show the results obtained using the proposed first level and second level MWT based DSR techniques and the existing enhancement methods for different dark gray images and colored images. Table 3 gives the values of performance metrics obtained by proposed technique and by existing techniques for different colored and dark gray images. Although the F, PQM and CEF values for histogram equalization, gamma correction, multi scale retinex and single scale retinex methods are higher, the visual qualities of the obtained enhanced images are not good. Figure 7 illustrates the bar graph representation of the performance metrics F, PQM, CEF and time taken for execution. The results imply that the use of the first level multi wavelet transform can give the same results as the one obtained with complex daubechies wavelet transform based DSR, which are better than other existing methods. The time and number of iterations required for obtaining the optimal enhanced results are less, compared to the CDWT-DSR and other solutions. The reason behind the reduction in computational complexity in MWT based DSR is due to the usage of more low frequency information, i.e., the availability of four low frequency sub bands in case of first level MWT decomposition and sixteen sub bands in case of second level MWT decomposition. The performance metrics acquired and computational complexity involved in the second level MWT based DSR are better compared with the first level MWT based DSR and others. The reason is again that more information is available in the approximation sub bands, and with less number of iteration F, the PQM converges.

In Fig. 7, metrics are compared for four more DSR based techniques, such as HEQ, Gamma Correction, MSR and Retinex. In addition, the comparison results for the benchmark gray level Lena and Peppers images are also given in Fig. 7. In Fig. 7(a), although the Contrast enhancement factor (F) values of House Image for Histogram Equalization Technique (HEQ), MSR and Retinex methods are high, compared to the proposed method, the PQM (only 4.9) is very low while the CEF is high for the HEQ method. Note that the CEF value for the MSR and Retinex is very low for the House image.

In Fig. 7(c), although the Color Enhancement Factor (CEF) value of House Image for the Histogram Equalization Technique (HEQ) is high, compared to other methods, the PQM is very low. This implies poor visual quality as obtained in our enhanced images. For the Sea settle and Foot-ball images, the proposed second level MWT-DSR generates superior results over other methods. From Fig. 7, it is apparent that although a few existing methods can attain greater values of F or CEF, they do so by compromising the visual quality. In this context, the results given in

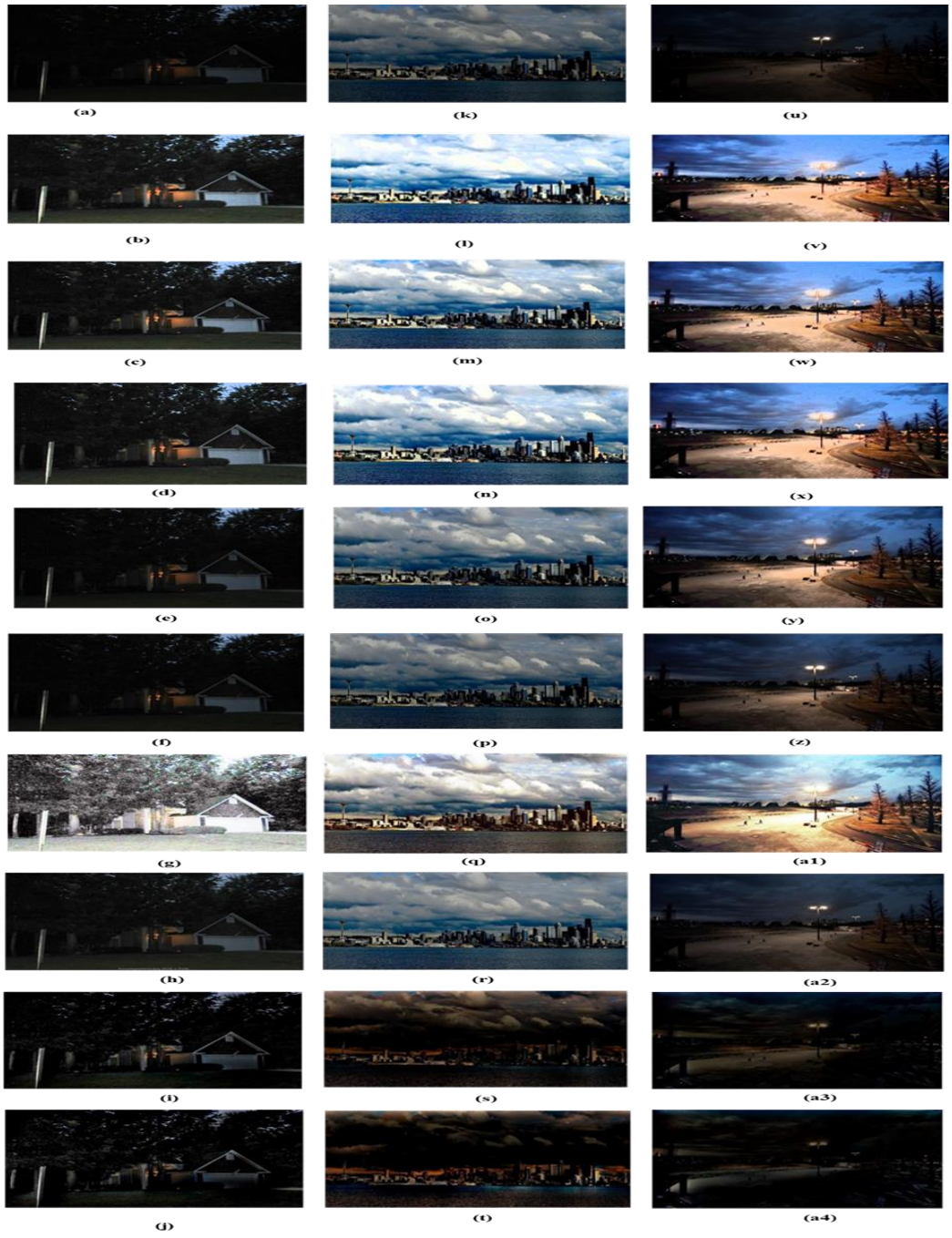

Figure 6. **Comparison of proposed method result with existing enhancement technique results for different color images. (a), (k), (u)- Input images, (b), (l), (v)- Second level MWT method, (c), (m), (w)- First level MWT technique, (d), (n), (x)- CDWT- DSR technique, (e), (o), (y)- DWT- DSR technique, (f), (p), (z)- DSR technique, (g), (q), (a1)- HEQ technique, (h), (r), (a2)- Gamma correction, (i), (s), (a3)- MSR, (j), (t), (a4)- SSR.**

Table 3. Performance comparison for different methods

Name of the method	Performance Metrics	House	Sea settle	Foot ball	Lena	Peppers
Second level MWT - DSR	F	2.14	1.85	3.601	12.2	5.72
	PQM	9.07	8.89	9.49	8.00	7.93
	CEF	3.23	2.67	6.87		
	No. of iterations	8	5	18	42	21
	Time taken for execution in Seconds	9.3	5.4	17.42	11.4	4.17
First level MWT- DSR	F	2.09	1.8	3.51	11.9	5.31
	PQM	8.43	8.2	9.18	8.8	9.18
	CEF	2.65	2.0	6.14		
	No. of iterations	27	16	63	50	69
	Time taken for execution in Seconds	27	14	53	15.5	11.48
CDWT-DSR	F	2.0	1.84	3.4	11.8	4.20
	PQM	9.7	8.93	9.8	8.9	8.17
	CEF	2.6	2.21	6.02		
	No. of iterations	61	35	150	68	100
	Time taken for execution in Seconds	94	44	225	18.7	38.08
DWT-DSR	F	1.36	1.34	2.8	8.9	3.72
	PQM	9.01	8.44	9.7	9	10.13
	CEF	1.42	1.40	4.0		
	No. of iterations	42	29	117	45	17
	Time taken for execution in Seconds	46.3	28	122	8.7	4.28
DSR	F	1.36	1.14	2.2	10.02	3.18
	PQM	9.9	9.78	10.9	9	10.48
	CEF	1.3	1.40	2.2		
	No. of iterations	42	29	117	45	14
	Time taken for execution in Seconds	60	35	93	5.91	1.48
HEQ	F	2.5	1.8	2.9	9.0	2.74
	PQM	4.9	8.2	9.0	8.5	9.72
	CEF	3.4	1.2	4.5		
	Time taken for execution in Seconds	3.16	1.92	1.82	1.18	1.29
Gamma Correction	F	0.99	0.93	1.1	3.6	2.22
	PQM	7.78	9.01	10.54	10.7	10.89
	CEF`	1.58	1.3	1.5		
	Time taken for execution in Seconds	2.0489	4.5017	2.086	2.086	4.3597
MSR	F	2.7	1.7	1.6	2.8	3.75
	PQM	8.1	9.6	11.3	8.7	10.59
	CEF	0.8	0.87	1.1		

Name of the method	Performance Metrics	House	Sea settle	Foot ball	Lena	Peppers
	Time taken for execution in Seconds	4.9402	3.6421	2.774	1.506	1.9047
Retinex	F	2.79	1.74	1.69	9.8	3.33
	PQM	8.1865	9.2	10.9	8.9	11.25
	CEF	1.29	0.872	1.151		
	Time taken for execution in Seconds	4.4123	3.6050	3.763	1.312	1.6013

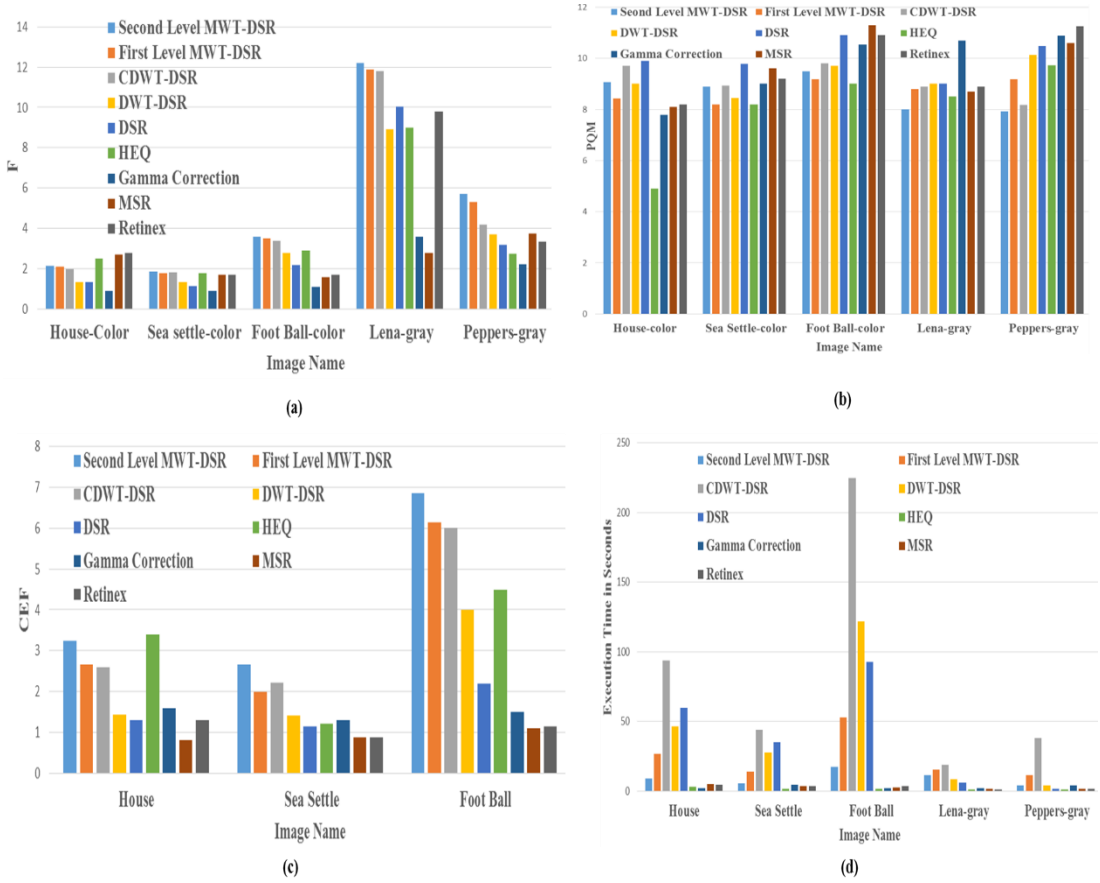

Figure 7. **Bar graph representation of performance metrics for different methods.**

Table 4. **Computations required for second level MWT-DSR, MWT-DSR and CDWT-DSR**

Name of the method	No. of multiplications	No. of additions
MWT DSR_SEC LEV	[M/4*N/4*5*64]*n	[M/4*N/4*3*64]*n
MWT DSR	[M/2*N/2*5*16]*n	[M/2*N/2*3*16]*n
CDWT DSR	[M/2*N/2*14*4]*n	[M/2*N/2*10*4]*n

Mukherjee and Mitra (2008), Wang, et al (2002) justify the effectiveness of our method.

The time taken for execution of the MWT based DSR is less compared with the first level MWT based DSR and CDWT based DSR. The number of iterations required for image enhancement is also less in the second level MWT based DSR, which results in reduction of number of multiplications and additions. If we consider an image of size M×N, the number of multiplications and additions for the second level MWT- DSR and the first level MWT- DSR and CDWT- DSR are given in Table 4 for the following system configuration: Processor: Intel (R) Core (TM) i3-4005U CPU @ 1.70GHz, Installed Memory (RAM): 4.00GB, System type: 64-bit Operating System, x64- based processor. The term 'n' in Table 4 represents the number of iterations. Although the time taken for execution of HEQ, Gamma correction, MSR and Retinex are less, and the visual quality provided by those techniques is very poor.

7 CONCLUSIONS

FROM the conducted exhaustive experiments, the results show that the Second level Multiwavelet transform based DSR gives better results in terms of performance metrics, when compared with the first level MWT-DSR and other existing techniques. The computational complexity and time required for execution in obtaining the results for the second level MWT-DSR are less, when compared with the first level MWT-DSR and CDWT-DSR. The reason is that for the second level MWT-DSR, the proposed method operates over more number of low frequency sub bands compared to the first level MWT-DSR, CDWT-DSR and DWT- DSR techniques. The GHM balanced MWT preserves the edges visually better, because the multiwavelet is simultaneously symmetrical and orthogonal and thereby reduces the Cartesian artifacts compared to the scalar wavelets.

8 ACKNOWLEDGMENT

THE authors express their gratitude to Mr. Sajan Pillai for providing images for testing the proposed technique. They also thank and acknowledge Ms. Rajlaxmi Chouhan for her valuable suggestions and supports. Xiao-Zhi Gao's research work was partially supported by the National Natural Science Foundation of China (NSFC) under Grant 51875113.

9 REFERENCES

R. Benzi, A. Sutera, and A. Vulpiani, (1981). The mechanism of stochastic resonance, *J. Phys. A.* 14, 453-457.

L. Bockstein, (1986). Color equalization method and its application to color image processing, J. Opt. Soc. Amer. 3(5), 735-737.

L. Gammaitoni, P. Hanggi and F. Marchesoni, (1998). Stochastic resonance, *Rev. Mod. Phys.* 70, 223-270.

T. C. Gard, (1998). Introduction to stochastic differential equations" (Marcel-Dekker, New York,).

R. C. Gonzales, & E. Woods (1992). *Digital Image Processing. Addison-Wesley*.

M. Hongler, Y. Meneses, A. Beyeler, and J. Jacot, (2003). Resonant retina: Exploiting vibration noise to optimally detect edges in an image, *IEEE Trans. Pattern Analysis and Machine Intelligence.* 25(9), 1051-1062.

Y. U. Huihui, J. I. Ronghua, L. I. Jingyuan and Tiantian Wang, (2012). Color image filtering methods for variable spray systems, Intelligent *Automation and Soft Computing.* 18(5), 453-460.

R. K. Jha, P. K. Biswas, and B. N. Chatterji, (2012). Contrast enhancement of dark images using stochastic resonance, *IET Journal of Image Processing.* 6, 230-237.

R. K. Jha, R. Chouhan, and P. K. Biswas, (2012). Noise-induced contrast enhancement of dark images using non-dynamic stochastic resonance, *In Proc. National Conference on Communications.* 1-5.

D. J. Jobson, Z. Rahman, and G. A. Woodell, (1997). Properties and performance of a center/surround retinex, *IEEE Trans. Image Process.* 6(3), 451-462.

D. J. Jobson, Z. Rahman and G. A. Woodell, (1997). A multi-scale retinex for bridging the gap between color images and the human observation of scenes, *IEEE Trans. Image Process.* 6(7), 965-976.

P. Jung, & P. Hanggi, (1991). Amplification of small signal via stochastic Resonance, *Phys. Rev. A.* 44(12), 8032-8042.

L. Ghouti, Ahmed Bouridane, Mohammad K. Ibrahim and Said Boussakta, (2006). Digital Image Watermarking Using Balanced Multiwavelets, *IEEE Transactions on Signal Processing.* 54(4), 1519-536.

J. S. Lim, (1990). Two-Dimensional Signal and Image Processing, *Englewood Cliffs, NJ: Prentice-Hall*.

J.-M. Lina, (1997). Complex Daubechies Wavelets: Filters design and applications, *in: Proceedings of 1st Conference of International Society for Analysis, its Applications and Computation.* 1-18.

J.-M. Lina & M. Mayrand, (2002). Complex Daubechies wavelets, *Applied and Computational Harmonic Analysis.* 2(3), 219-229.

J. Mukherjee, & S. K. Mitra, (2008) Enhancement of color images by scaling the DCT coefficients, *IEEE Transactions on Image Processing.* 17(10), 1783-1794.

R. Peng, H. Chen, and P. K. Varshney, (2007). Stochastic resonance: An approach for enhanced medical image processing, *In IEEE/NIH Life Science Systems and Applications Workshop.* 1, 253-256.

C. Rajlaxmi, C. Pradeep Kumar, Rawnak Kumar and Rajib Kumar Jha, (2012). Contrast Enhancement

of Dark Images Using stochastic Resonance in Wavelet Domain, *International Journal of Machine learning and computing.* 2(5), 711-715.

C. Rajlaxmi, Rajib Kumar Jha and Prabir Kumar Biswas, (2012). Enhancement of dark and low-contrast images using dynamic stochastic resonance, *IET Image Processing.* 7(2), 174-184.

C. Rajlaxmi, Rajib Kumar Jha and Prabir Kumar Biswas, (2012). Wavelet-based Contrast Enhancement of Dark Images using Dynamic Stochastic Resonance, *Proceedings of the Eighth Indian Conference on Computer Vision, Graphics and Image Processing (ICVGIP'12).*

V. P. S. Rallabandi, (2008). Enhancement of ultrasound images using stochastic resonance based wavelet transform, *Computerized medical imaging and graphics.* 32, 316-320.

V. P. S. Rallabandi & P. K. Roy, (2010). Magnetic resonance image enhancement using stochastic resonance in Fourier domain, *Magnetic Resonance.* 28, 1361-1373.

R. M. Rao, & A. S. Bopardikar, (2000). Wavelet Transform-Introduction to Theory and Applications, *Pearson Education Inc.*

H. Risken, (1984). *The Fokkar Plank equation, Springer Verlag, Berlin.*

C. Ryu, S. G. Konga, and H. Kimb, (2011). Enhancement of feature extraction for low-quality fingerprint images using stochastic resonance, *Pattern Recognition Letters.* 32(2), 107-113.

H. Seddik, Sondes Tebbini and Ezzeddine Ben Braiek, (2014). Smart real time adaptive gaussian filter supervised neural network for efficient gray scale and RGB image denoising, *Intelligent Automation and Soft Computing.* 20(3), 347-364.

I. E. Selesnick, (2000). Balanced Multiwavelet Bases Based on Symmetric FIR Filters, *IEEE Transactions on Signal Processing.* 48(1), 184-191.

E. Simonotto, M. Riani, S. Charles, M. Roberts, J. Twitty, and F. Moss, (1997). Visual perception of stochastic resonance, *Phys. Rev. Lett.* 78(6), 1186-1189.

V. Strela, (1996). Multiwavelets Theory and Applications, *Moscow Institute of Physics and Technology.*

V. Strela, P. N. Heller, G. Strang, P. Topiwala and C. Heil, (1999). The Application of Multiwavelet Filter Banks to Image Processing, *IEEE Trans. on Image Processing.* 8(4), 1-30.

R. N. Strickland, C. S. Kim, and W. F. McDonnell, (1987). Digital color image enhancement based on the saturation component, *Opt. Eng.* 26(7), 609-616.

J. Tang, E. Peli, and S. Acton, (2003). Image enhancement using a contrast measure in the compressed domain, *IEEE Signal Process. Lett.* 10(10), 289-292.

Z. Wang, H. R. Sheikh, and A. C. Bovik, (2002). No-reference perceptual quality assessment of jpeg compressed images, *In Proc. IEEE Int. Conf. Image Processing.* 1, 477-480.

S. Wolf, R. Ginosar, and Y. Zeevi, (1998). Spatio-chromatic image enhancement based on a model of human visual information system, *J. Vis. Commun.* 9(1), 25-37.

Q. Ye, H. Huang, and C. Zhang, (2004). Image enhancement using stochastic resonance, *In Proc. IEEE Int. Conf. Image Processing.* 1, 263-266.

Q. Ye, H. Huang, X. He and C. Zhang, (2003). A SR-based radon transform to extract weak lines from noise images, *Proc. IEEE Int. Conf. on Image Processing, Barcelona, Spain.* 5(6), 1849-1852.

10 NOTES ON CONTRIBUTORS

S. Deivalakshmi is currently working as a Professor in the Department of ECE, National Institute of Technology, Tiruchirappalli, India. Her research interests include Multi resolution based Image de-noising and Enhancement techniques, Deep learning based image restoration and Medical image analysis. She has published research papers in refereed international journals and conferences.
Email: deiva@nitt.edu

P. Palanisamy is currently working as a Professor in the Department of ECE, National Institute of Technology, Tiruchirappalli, India. His research interests include Statistical Signal Processing, Adaptive and Array Signal Processing, Signal Detection and Parameter Estimation and Image Processing. He has published research papers in refereed international journals and conferences.
Email: palan@nitt.edu

Xiao-Zhi Gao has been appointed as a professor at University of Eastern Finland, Kuopio, Finland since 2018. He has published over 350 papers on refereed journals and conferences, and his Google Scholar H-index is 30. His research interests are nature-inspired computing methods with applications in optimization, data mining, machine learning, control, and industrial electronics.
Email: xiao.z.gao@gmail.com